JOURNAL OF MATERIALS SCIENCE 31 (1996) 4837–4842

Layered Si_3N_4 composites with enhanced room temperature properties

P. ŠAJGALÍK, Z. LENČÉŠ
Institute of Inorganic Chemistry, Slovak Academy of Sciences, Dúbravská cesta 9, SK-842 36 Bratislava, Slovakia

J. DUSZA
Institute of Materials Research, Slovak Academy of Sciences, Watsonova 47, SK-043 53 Košice, Slovakia

Four silicon nitride multilayer composites were prepared by hot pressing. Internal stress distribution along the layer boundary dictates the anisotropy of mechanical properties of the composite. The room-temperature bending strength and fracture toughness of all layered composites was higher than the bending strength of related monoliths. Layered ceramic materials exhibited higher tolerance to flaws in comparison to the monolithic ceramic.

1. Introduction

The potential of Si_3N_4-based ceramics/composites with respect to the mechanical properties is still not exhausted. A great effort to improve these properties is being made, and quite promising achievements have been reached in this field in recent years. The room temperature strength > 1 GPa, is not exceptional; fracture toughness > 10 MPa $m^{1/2}$ and Weibull modulus higher than 40 were also reported [1–5]. All these property improvements were achieved by more sophisticated processing of Si_3N_4 ceramics/composites, based on the better knowledge of basic phenomena accompanying the silicon nitride densification. Weakening the bonds between grain boundary and Si_3N_4 grains to the appropriate level and extension of the crack path by the presence of either elongated Si_3N_4 grains or the creation of subgrain boundaries (by introduction of inclusions, e.g. SiC subgrains, [5]) were the base for these substantial improvements of room- as well as high-temperature properties.

Because of the validity of Griffith's equation, these materials are extremely sensitive to the flaw-size distribution. Large flaws have catastrophic consequences on the strength and reliability. In our previous work [6] it was shown that by decreasing the maximum flaw size from approximately 80 μm to 20–30 μm (which was, in fact, the size of the largest grains), the four-point bending strength was increased from 512 MPa to 930 MPa.

The above-mentioned requirement on grain-boundary engineering on the micro-nano-level and the production of flaw-free materials, puts extreme requirements on the processing of Si_3N_4-based materials with enhanced mechanical properties. It is generally known that Si_3N_4-based ceramics/composites with different micro-nano-structures react to the propagating crack differently. The microstructural characteristics for Si_3N_4 ceramics are in contradiction: extremely tough material with a coarse microstructure and high-strength material with a fine microstructure, respectively [7]. These facts lead to the idea of preparing Si_3N_4 composites with layers of different microstructure [8, 9], similar to the recently reported oxide ceramic materials with a layered microstructure, which exhibit a significant improvement in fracture toughness, strength and tolerance to the flaws [10, 11]. In layered materials, the new boundaries (potential barriers for propagating crack and dissipaters of crack-tip energy) are realized on the milli-level and so microstructure boundary engineering is not accompanied by the substantially increased requirements of the processing.

The present paper reports the preparation of Si_3N_4 composites with layered structure. The room-temperature mechanical properties of layered composites, as well as the monolithic ceramic materials, of which the layered materials are consisted, are compared. The role of the boundary between the microstructure layers is studied and discussed on the basis of the simplified energetic model of the crack.

2. Experimental procedure

The starting mixtures were prepared by attrition milling of Si_3N_4 powder with sintering aids in dry isopropanol for 4 h in the weight ratios listed in Table I. The layers of starting powder mixtures were pressed by the uniaxial pressure of 200 MPa in the desired succession. The green pellets were hot-pressed at temperatures ranging from 1750–1850 °C and mechanical pressure of 30 MPa. The furnace atmosphere was either nitrogen or a vacuum. Discs, of 50 mm diameter and 4.5 mm height, with the 99% theoretical density, were cut into bars (3 mm × 4 mm × 45 mm) with the tensile face (15 μm finish) perpendicular to the

0022–2461 © *1996 Chapman & Hall*

TABLE I Starting powders composition

Starting powder mixture	Si_3N_4 (wt %)	Sintering aids (wt %)			Microstructure forming and reinforcing powders (wt %)			
		Al_2O_3	Y_2O_3	La_2O_3	Amorph. Si_3N_4	Equiaxed β-Si_3N_4	Amorph. SiNC	SiC_{pl}
A	72[a]	3.4[b]	4.6[c]	–	–	20[d]	–	–
B	72[a]	3.4[b]	4.6[c]	–	20[e]	–	–	–
C	74[f]	–	3.0[g]	3.0[h]	–	–	–	20[i]
D1	73[f]	2[j]	5[g]	–	–	–	20[k]	–
D2	72[a]	3.4[b]	4.6[c]	–	–	–	20[k]	–
E	93[f]	2[j]	5[g]	–	–	–	–	–

[a]LC-12-S, H.C. Starck, Germany. [f]UBE SNE10, Japan. [b]Fluka AG, Germany. [j]Alcoa A16. [c]Techsnabexport, Russia. [g]H.C. Starck, Germany. [h]Merck, Darmstadt, Germany. [e]Prepared in house. [d]SHS powder prepared in the Institute of Macrokinetics, Chernogolovka, Russia. [i]C-Axis Technology, Canada. [k]CISE, Italy.

hot-pressing direction. The bending strength was evaluated using a four-point bending fixture with inner/outer span 20/40 mm and a crosshead rate of 0.5 mm min^{-1}. The indentation strength in bending (ISB) fracture toughness was calculated from the results of strength determined on specimens with the dimensions 3 mm × 4 mm × 25 mm and broken in three-point bending mode after indentation with a load of 294 N. The ISB method was used for determination of the fracture toughness of whole composites and monoliths. Indentation fracture (IF) toughness was calculated using the formula given by Shetty *et al.* [12]. The IF method was used for evaluation of the fracture toughness of individual layers. Microstructures were observed on the polished and plasma-etched surfaces by SEM. The five different composites with layered structure are discussed in the present paper. Each consists of only a couple of layers which are repeated differently for different composites. The composites are denoted according to the starting mixtures listed in Table 1, followed by the total number of layers in brackets, e.g. a composite consisting of four alternating layers of starting compositions A and B is denoted A–B(4).

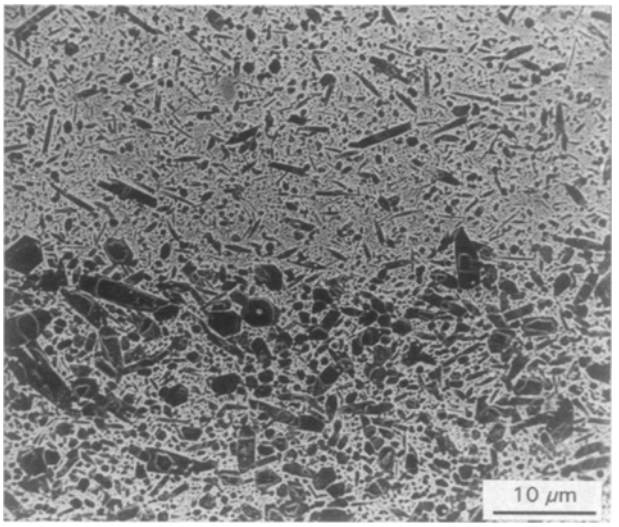

Figure 1 Micrograph of two adjacent layers with different microstructure. The layer boundary exhibits no structural defects.

3. Results

3.1. Structure of layered composites

An example of a layered structure is shown in Fig. 1. The layer boundary is sharp and well visible. No technological defects or microstructural inhomogenities were found at the layer boundaries.

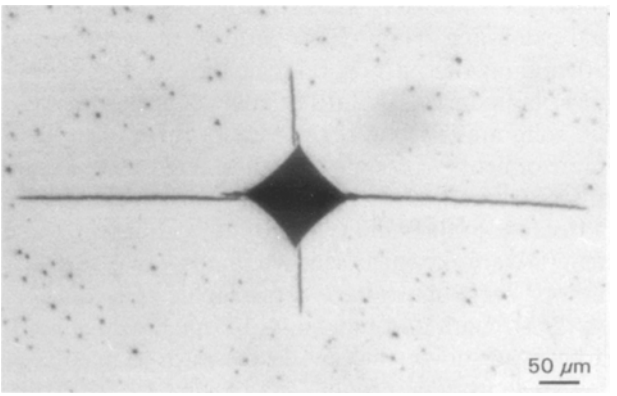

Figure 2 Vickers' indent with different lengths of cracks parallel and perpendicular to the layer boundary.

3.2. Crack length and fracture toughness anisotropy

The length of cracks introduced by a Vickers indentor into the particular layers of composites were measured. The difference in length of the cracks propagating parallel and perpendicular to the boundary between the layers with different microstructure were observed for all composites under study. Fig. 2 shows an example of such a behaviour. From these measurements the indentation fracture toughness (IFT) was evaluated. $K_{IC,\,paral.}$ is the fracture toughness evaluated from cracks parallel to the layer boundary, and $K_{IC,\,perp.}$ corresponds to the cracks perpendicular to the layer boundary. Fig. 3 shows the values of such measurements for two composites, A–B(4) and A–D2(7). Perpendicular IFT values are, in all cases, higher and the difference in these values is highest for layer A in the vicinity of layer B: 37%. The difference is

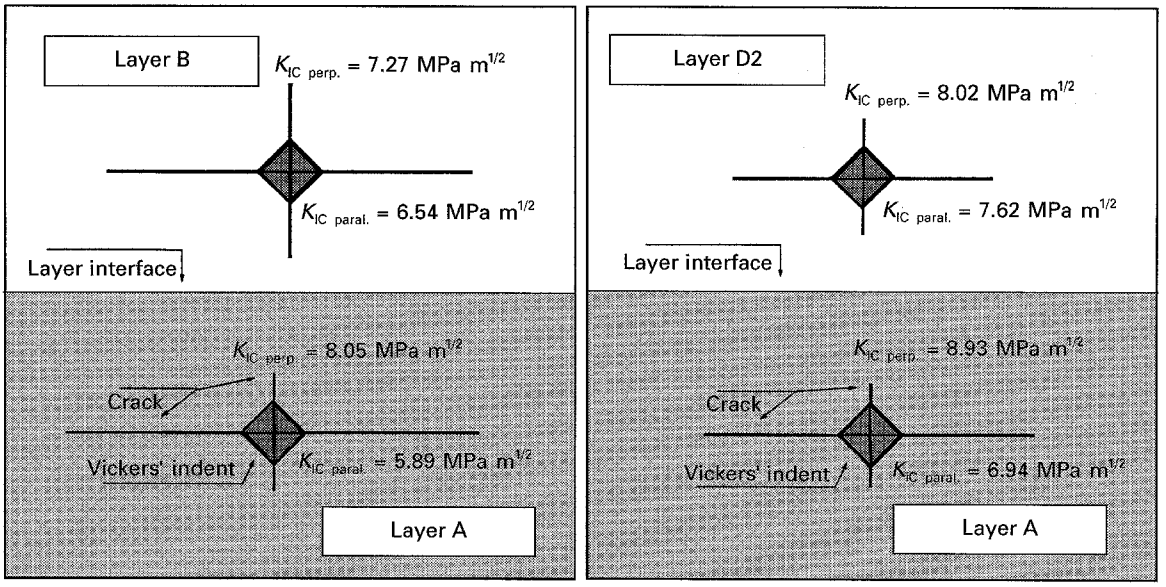

Figure 3 Fracture toughness anisotropy.

smallest for layer A in the vicinity of layer D2: only 5%. This difference in values indicates the strong internal stress anisotropy within the layers. The neighbouring layer influences the properties of the particular layer and plays a decisive role for influencing the residual stresses in this layer. This is documented by different IFT values for layer A in the vicinity of either layer B or layer D2, Fig. 3.

3.3. Interaction of the crack and the micro-nano-structure boundary

Vickers' cracks crossing the boundary are shown in Figs 4 and 5. Fig. 4 shows that the crack crossing the boundary is shorter than the crack propagating within the layer. The crack shown in Fig. 5 is deflected after crossing the microstructure boundary. This effect of crack deflection was also observed on bars broken in the four-point bending test. Fig. 6a shows the two pieces of broken bar put together and arrows indicate the deflection of the crack on the microstructure layers. The crack originally perpendicular to the tensile surface is almost parallel to this surface after several deflections. Fig. 6b schematically shows that the direction of the crack deflection at the layer boundary (angles α_1 and α_2) depends on the stress state of the following layer.

3.4. Fracture toughness and bending strength

The ISB fracture toughness and four-point bending strength values for monoliths as well as for layered composites are shown in Tables II and III. The fracture toughness and bending strengths of layered materials are, in all reported cases, higher than those for monoliths.

3.5. Fracture behaviour and flaw tolerance

In the all tested ceramic materials, hard agglomerates introduced from the starting powders are determined

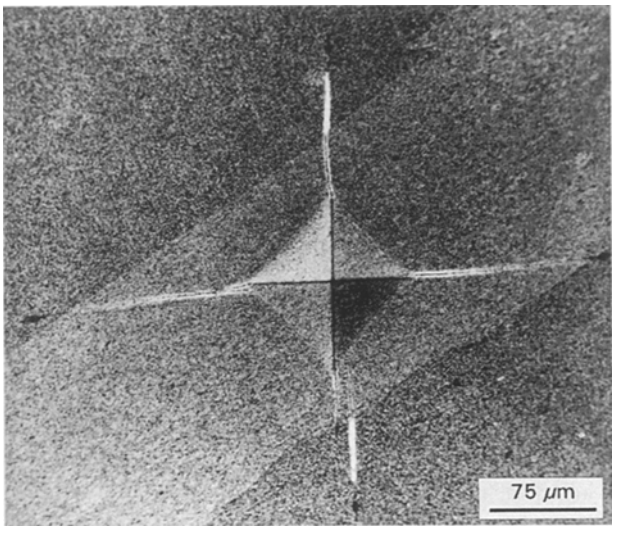

Figure 4 Vickers' indent with different lengths of cracks crossing the layer boundary and within one layer.

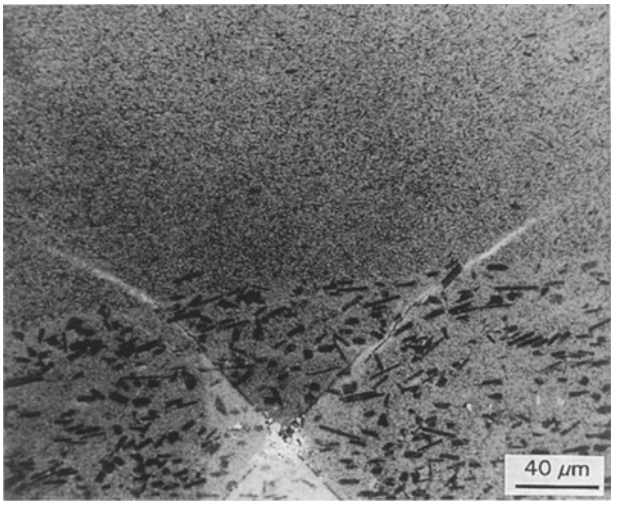

Figure 5 Interaction of the crack with the layer boundary, crack deflection.

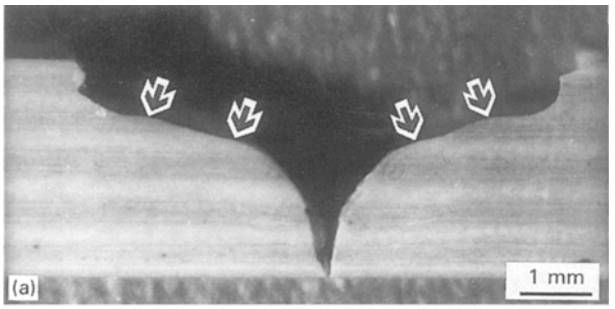

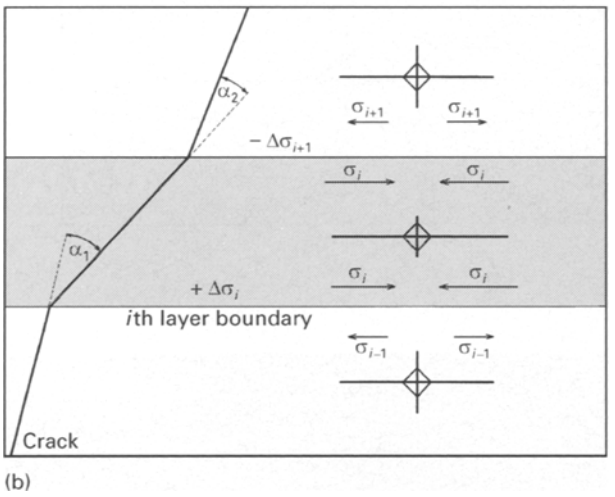

Figure 6 (a) Fragments of testing bar from the composite E–D1(12) after the four-point bending test. (b) Schematic illustration of crack deflection during the bending test and stress anisotropy on the layer boundaries.

TABLE II Mechanical properties of monolithic ceramics

	A	B	C	D1	D2	E
Bend strength (MPa)	640	615	622	–	640	720
K_{IC}(ISB) (MPa $m^{1/2}$)	6.9	6.1	–	–	6.6	–

TABLE III Mechanical properties of layered composites

	A–B(4)	E–D1(12)	A–D2(7)	C–E(3)
Approx. layer thickness (mm)	1	0.33	0.45	C = 0.7, E = 1.3, C = 2
Bend strength (MPa)	785	830	695	822
K_{IC}(ISB) (MPa $m^{1/2}$)	7.3	–	7.2	–

as the fracture origins. Fig. 7a shows a flat fracture surface of a monolithic material; the fracture origin is indicated by an arrow. The size of these agglomerates changes from 30 μm to 90 μm. The large defects, present in both materials (monoliths and composites), result in moderate bending strengths of monoliths, Tables II and III. Fig. 7b shows the fracture surface of a multilayer composite, this is much rougher, and the crack deflection on the structural layer is obvious. The upper layer delamination was observed during the

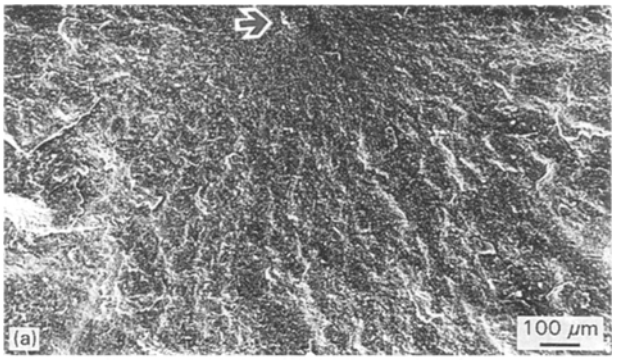

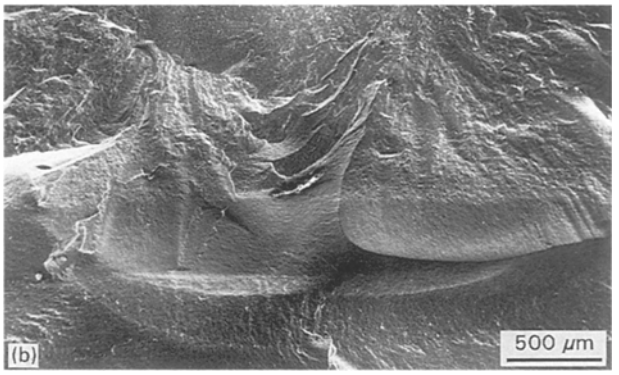

Figure 7 (a) The arrow shows the fracture origin and the fracture surface of the monolith material A. (b) Fracture origin and the fracture surface of the layered composite A–D2(7).

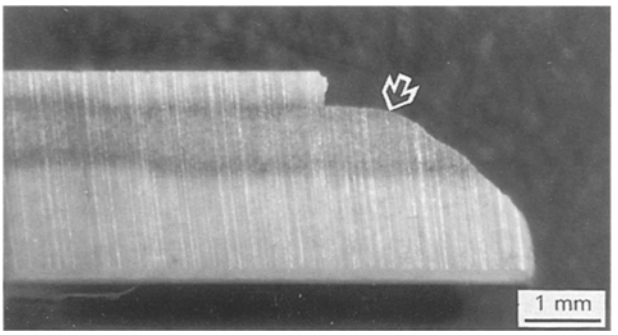

Figure 8 Fragment of testing bar from the composite C–E(3). The arrow indicates the delamination of the upper layer.

four-point bending test. It was observed that layer delamination starts at a load of approximately 70% of the critical one. Fig. 8 shows a broken bar with a delaminated layer. As a consequence of this effect, deviation from linearity in the load–displacement curve was observed, as is schematically shown in Fig. 9. All these mentioned phenomena result in a higher flaw tolerance of multilayer composites.

4. Discussion

4.1. Role of the layer boundary

As shown in previous paragraphs, the layer boundary significantly influences the fracture behaviour and mechanical properties of the composite. The role of the layer can be described according to the schematic illustration shown in Fig. 10. It is supposed that the crack is a result of tangential stress, σ_{t2}, acting on the crack in layer 2 which propagates from layer 2

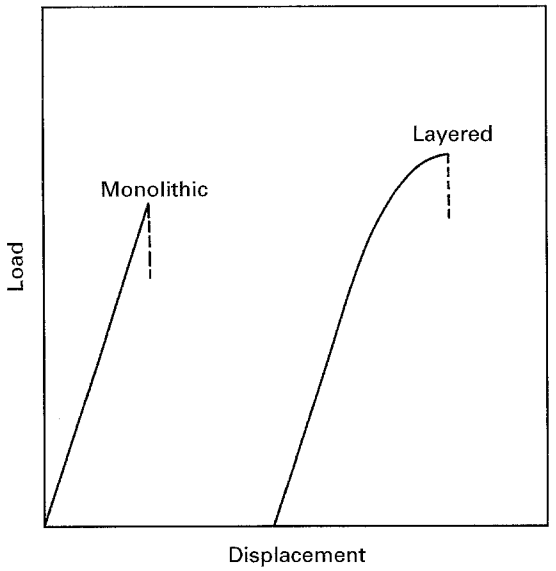

Figure 9 Schematic load–displacement curves for monolith and layered composites.

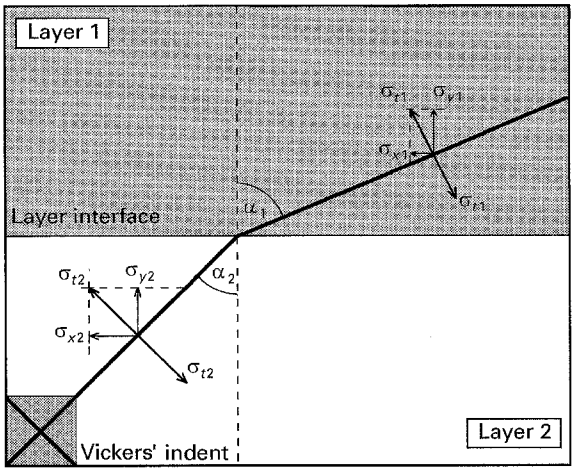

Figure 10 Schematic illustration of the crack propagating through two adjacent layers. Each layer is characterized by the different state of stress, σ_{t1} and σ_{t2}.

towards layer 1. The crack approaches the layer boundary under the angle α_2. Layer 1 is characterized by the stress, σ_{t1}. The difference between stresses σ_{t2} and σ_{t1} caused the crack deflection and the crack propagates further under the angle α_1. The kinetic energy, E_k, of the parts displaced by the advance of the crack is [13]

$$E_k = k\rho v^2 c^2 \sigma_t / 2E^2 \quad (1)$$

where k is a constant, ρ is the density, v is the brittle crack velocity, $2c$ is the length of the crack and E is the Young's modulus. In present calculation it is supposed that the difference between E_{k1} and E_{k2} is caused by the layer boundary. The maximum crack velocity can be expressed [13] by

$$v_{max} = (2\pi E/k\rho)^{1/2} \quad (2)$$

Substituting the crack velocity in Equation 1 by Equation 2, and subtracting E_{k2} and E_{k1}

$$\Delta E_k = E_{k2} - E_{k1} \quad (3)$$

one obtains the energy difference, ΔE_k, caused by the presence of a layer boundary. In the present approach it is considered that $c_1 = c_2$, i.e. that in the considered unit volume the crack length is approximately the same in layers 1 and 2, respectively. Then Equation 3 takes the form

$$\Delta E_k = E_{k2}(1 - \sigma_{t2}^2 E_2/\sigma_{t1}^2 E_1) = \chi E_{k2} \quad (4)$$

From Equation 4, the following conclusion can be drawn: the energy of the crack tip (propagating from layer 2 to layer 1) is consumed by the boundary in the case where the term in parentheses, marked as χ, is positive, $\chi > 0$. On the other hand, the crack is supplied by energy released from the boundary in the case where $\chi < 0$ (crack propagates from layer 1 to layer 2) and, finally, in the case where $\chi = 0$, the boundary does not influence the propagating crack. The ratio of Young's modulus and the ratio of internal stresses of both adjacent layers determine the energetic status of the boundary. The direction of the crack propagating through the boundary between layers 1 and 2 or vice versa determines the energy consumption/release mode.

4.2. Strength of the layered composite

This simplified kinetic energy model allows an understanding of the energetic status of the composite during the bending strength test. The energy necessary for the composite fracture can be extended or diminished by the presence of internal stresses. Increase or decrease of fracture energy is dependent on the direction from which the crack approaches the layer boundary, as was shown above. Applying this approach for bending strength, the total strength of the layered material can be expressed as follows

$$\sigma_{total} = \sigma_{comp.} + \sum_i \Delta\sigma_i \quad (5)$$

where σ_{total} is the measured bending strength, $\sigma_{comp.}$ is the strength of the internal stress-free layered composite and $\Delta\sigma_i$ is the difference of internal stresses in the adjacent layers, i.e. $\Delta\sigma_i = \sigma_i - \sigma_{i-1}$ is the internal stress of the ith layer boundary. This stress difference is defined by the equation [14]

$$\Delta\sigma = \frac{E_1 E_2(\beta_2 - \beta_1)\ (d_1 + 2d_2)\ \Delta T}{(1 - \nu_1)\ E_2 d_2 + (1 - \nu_2)\ E_1 d_1} \quad (6)$$

where ν is Poisson's ratio, E the Young's modulus, d the layer thickness, $\Delta T = T_j - T_0$, the temperature difference between T_j (temperature of rigid joints formation between the layers) and room temperature, T_0. Total dimensional change of the particular layer as a result of sintering is given by contributions from thermal expansion and sintering, thus $\Delta l/l_0 = (\Delta l_t + \Delta l_s)\ /l_0 = (\beta_t + \beta_s)\ \Delta T = \beta\Delta T$, i.e. coefficient β is determined by the thermal expansion coefficient of the matter and by the shrinkage of the appropriate layer. The positive or negative contribution of $\Delta\sigma$ to σ_{total}, Equation 5 depends on the value of β_1 and β_2 of two adjacent layers. In the case when $\beta_1 < \beta_2$, its contribution is positive, and in the case when $\beta_1 > \beta_2$,

it is negative. Thus, the measured bending strength changes with respect to the sign of $\Delta\sigma_i$. The scheme is shown in Fig. 6b.

According to Equation 6, the influence of layer thickness, d, on $\Delta\sigma$ is most favourable, when the thickness of the layer under compression is much higher than that under tensile stress. Because the matrix of all layers is based on silicon nitride, the influence of E and ν of particular layers on $\Delta\sigma$ is not so strong. If the second matrix is different, e.g. TiN, the influence of these parameters will be much higher.

The conclusions mentioned above can be applied to the explanation of the results obtained for material A–B. The four-point bending strength of the four-layer composite A–B(4) consisting of fine and coarse Si_3N_4 layers, respectively, with the tensile surface of a coarse layer is 785 $\pm$ 83 MPa (this value is reported in Table III). In the case, when the fine Si_3N_4 is on the tensile surface, this value is only 630 $\pm$ 107 MPa (this value is not reported in Table III). This fact can be qualitatively explained by a previous energetic approach. In the case of higher bending strength, two of the three layer boundaries contribute positively ($\Delta\sigma_1 + \Delta\sigma_3$) to the composite strength, $\sigma_{comp.}$, and one negatively, $-\Delta\sigma_2$. In the case of lower bending strength, two boundaries contribute negatively, $-\Delta\sigma_1 - \Delta\sigma_3$ and only one positively, $+\Delta\sigma_2$. When the composite consists of seven layers, i.e. with three boundaries positively contributing to the fracture energy and three boundaries contributing negatively, the four-point bending strength of such a composite was 730 $\pm$ 71 MPa, independently of the positioning of the sample with respect to the layer sequence during the bending test.

4.3. Flaw tolerance

A possible explanation of the higher bending strength measured for the layered composites was given in the previous paragraph. The stress of the boundary layer, in this case positive with respect to Equation 5, diminishes the maximum stress acting on the flaw. Thus, Griffith's law is not applicable for the layered composite. The positive boundary stress acts as a shield for the flaw, and so the layered material is more flaw tolerant than the monolithic one.

5. Conclusion

1. Anisotropy of the length of Vickers' cracks documented the presence of different internal stresses within the layers of the composite.

2. Crack deflection on the layer boundary is a result of the presence of these different stresses along the boundary.

The internal stresses, as a consequence of the existence of layer boundaries in the layered composites, cause the higher room-temperature bending strength and larger flaw tolerance of these materials.

Acknowledgements

P. Šajgalík acknowledges the Alexander von Humboldt Foundation for financial support during his stay at the Max-Planck-Institut für Metalforschung, Pulvermetallurgisches Laboratorium, Stuttgart, Germany, where part of this work was carried out. Z. Lenčéš acknowledges the Research Institute for Ceramic Technology, Faenza, Italy where part of this work was also carried out. This work was also partly financed by Slovak Grant Agency under the contract number 2 1169 94 .

References

1. W. DRESSLER, PhD Thesis, Universität Stuttgart, Germany (1993).
2. W. DRESSLER, M. J. HOFFMANN and G. PETZOW, in "Proceedings Silicon Nitride 93", edited by M.J. Hoffmann, P. F. Becher and G. Petzow, "Key Engineering Materials", vol. 89–91 (Trans Tech Publications, Aedermannsdorf, 1994) p. 165.
3. M. J. HOFFMANN, in "Proceedings of the NATO Advanced Research Workshop on Tailoring of Mechanical Properties of Si_3N_4 Ceramics", edited by M. J. Hoffmann and G. Petzow, *NATO ASI Series* vol. 276 (Kluwer Academic, Dordrecht, Boston, London, 1994) p. 59.
4. P. F. BECHER, S. L. HWANG, H. T. LIN and T. N. TIEGS, *ibid.*, p. 87.
5. K. NIIHARA, Ceram. Soc. Jpn **100** (1992) 536.
6. P. ŠAJGALÍK and J. DUSZA, in "Euro-Ceramics II", vol. 2, "Structural Ceramics and Composites", edited by G. Ziegler and H. Hausner (Deutsche Keramische Gesellschaft e.V., Kóln, 1993) p. 1589.
7. P. F. BECHER, *J. Am. Ceram. Soc.* **74** (1991) 222.
8. P. ŠAJGALÍK, Z. LENČÉŠ and J. DUSZA, in "Ceramic Materials and Composites for Engines", edited by D. S. Yan, X. R. Fu and S. X. Shi (World Scientific, Singapore-New Jersey-London-Hong Kong, 1995) p. 198.
9. P. ŠAJGALÍK, J. DUSZA and Z. LENČÉŠ, in "Ceramic Processing Science and Technology", edited by H. Hausner, G. L. Messing and S. Hirano, *Ceramics Transactions*, vol. 51, (The American Ceramic Society, Westerville, Ohio, 1995) p. 603.
10. M. P. HARMER, H. M. CHAN and G. A. MILLER, *J. Am. Ceram. Soc.* **75** (1992) 1715.
11. D. B. MARSHALL, J. J. RATTO and F. F. LANGE, *ibid.* **74** (1991) 2979.
12. D. K. SHETTY, I. G. WRIGHT, P. N. MINCER and A. H. CLAUER, *J. Mater. Sci.* **20** (1985) 1873.
13. N. J. PETCH, in "Fracture – An Advanced Treatise", vol. I, "Microscopic and Macroscopic Fundamentals", edited by H. Leibowitz (Academic Press, New York, London, 1968) p. 361.
14. T. CHARTIER, D. MERLE and J. L. BESSON, *J. Eur. Ceram. Soc.* **15** (1995) 101.

Received 28 March 1995
and accepted 13 February 1996